

Electronic Supplementary Information

Cyclic Strain Enhances the Early Stage Mineral Nucleation and the Modulus of Demineralized Bone Matrix

Doyoon Kim^{1,‡}, Byeongdu Lee², Brittany Marshall³, Stavros Thomopoulos³, and
Young-Shin Jun^{1,*}

¹*Department of Energy, Environmental & Chemical Engineering, Washington University in
St. Louis, St. Louis, Missouri 63130, United States*

²*X-ray Science Division, Argonne National Laboratory, Argonne, Illinois 60439, United
States*

³*Department of Orthopedic Surgery, Department of Biomedical Engineering, Columbia
University, New York, New York 10032-3072, United States*

***To Whom Correspondence Should be Addressed**

Address: One Brookings Drive, Campus Box 1180

E-mail: ysjun@wustl.edu

<http://encl.engineering.wustl.edu/>

Biomaterials Science

[‡]Current address: Department of Civil and Environmental Engineering, Massachusetts Institute of
Technology, Cambridge, MA 02139, USA

Summary: Total 16 Pages, including 10 Figures and 2 Tables

Supporting Note: Small-angle X-ray scattering and wide-angle X-ray diffraction data collection and analysis

Small-angle X-ray scattering (SAXS) data were collected for collagen matrices during *in situ* calcium phosphate mineralization at the Advanced Photon Source (APS) sector 11-ID-B of Argonne National Laboratory (IL, USA). The sample holder grip module was designed to be detached from the BiSlide machine during mineralization, and to be loaded on another modularized sample stage for the SAXS measurement (Fig. S1a–c). For each SAXS scan, the sample was exposed to a 13.3 keV X-ray beam for 1 second. The sample was scanned five times, moving the sample stage vertically by 0.2 mm per scan. The average intensity value of five scans was taken to represent one position of the sample. The left half and the right half of each sample (total 10 scans) were measured at each time interval (Fig. S1d). From the obtained 2-dimensional scattering intensity images, 1-dimensional scattering intensities, $I(q)$, were extracted by averaging the sector along the horizontal direction, which was perpendicular to the fibrillar direction (Fig. S1d). Therefore, we were able to analyze $I(q)$ to quantify the nucleation rates and to obtain the morphology of newly formed particles without interference by peaks caused by the periodicity (~67 nm) of the collagen gap and hole regions. The distance from the sample to the SAXS detector (Pilatus 2M) was 2 m, which provided a range of 0.003–0.5 Å⁻¹ for the scattering vector, q . Silver behenate powder was used as the q calibration standard, and $I(q)$ was normalized by the incident beam intensities and calibrated using a reference glassy carbon standard sample.¹ In this way, SAXS intensities collected from different measurements could be compared.

Further SAXS data analyses were conducted using 1-dimensional intensity data. Total particle volume was estimated from the linear relationship with invariant values, $Q = \frac{1}{2\pi^2} \int q^2 I(q) dq$. Due to the relatively high noise in the large q regions, integration was conducted only within a limited q range of 0.005–0.3 Å⁻¹. The Modeling II tool of the IRENA package written in IGOR Pro (WaveMetrics Inc.) was provided by APS and used to fit the SAXS pattern to evaluate the particle morphologies and volume fractions. Details about the models used in the package are well described elsewhere.²

Similarly, to identify CaP phases during collagen mineralization, *in situ* wide-angle X-ray diffraction (WAXD) data was collected at APS sector 11-ID-B. Every two hours during the mineralization, collagen samples were exposed to a 58.66 keV X-ray beam for 10 seconds, with a 95 cm distance between the sample and detector (Perkin Elmer amorphous silicon detector). Due to the larger beam size (500 μm × 500 μm) and longer exposure time for WAXD than for SAXS, a one-time scan was used to collect the data for one spot. Because the peaks generated from collagen periodicity do not appear in the q range of the WAXD analysis, the 2-dimensional intensities were then averaged over the q range along the radial direction to produce 1-dimensional intensities $I(q)$, using GSAS-II.³ Cerium dioxide was used as the calibration standard.

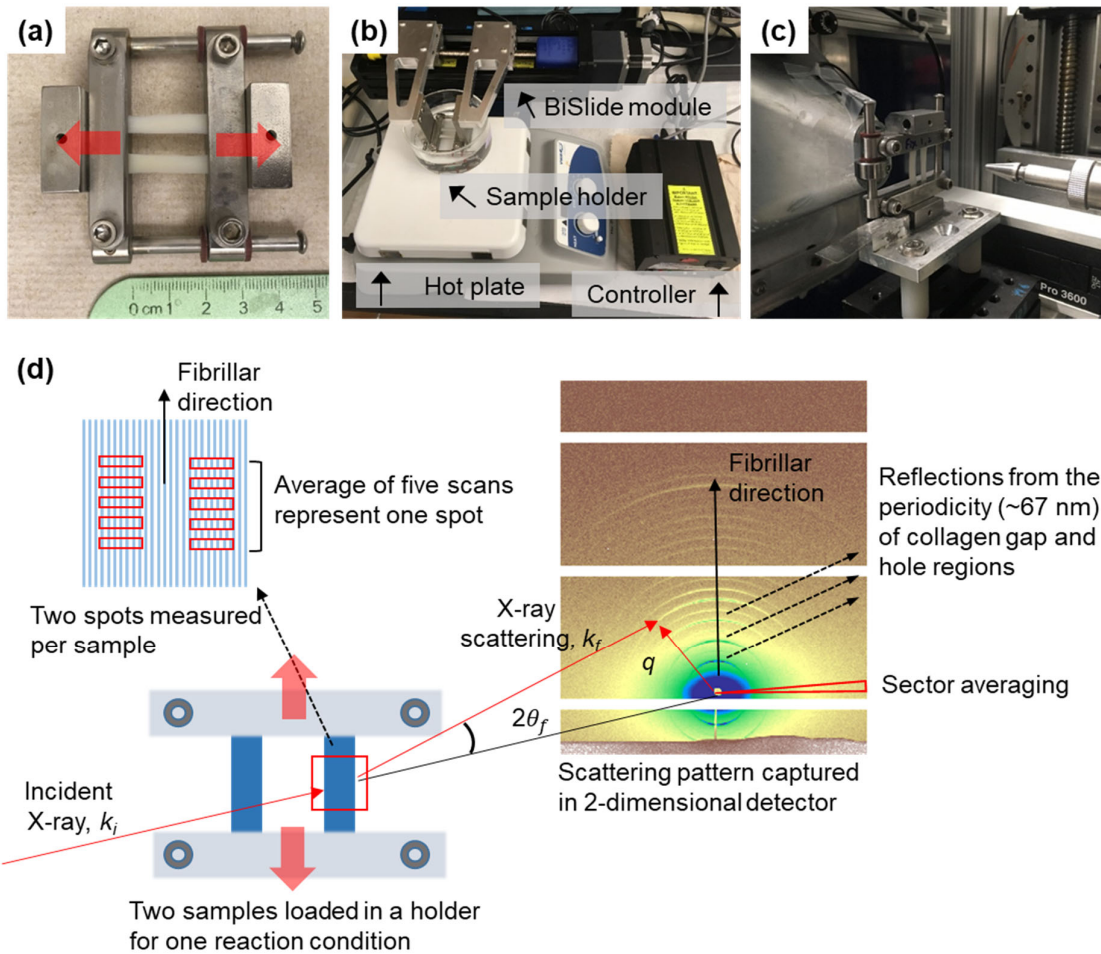


Figure S1. Experimental setup for *in situ* collagen mineralization. a) A custom-made stainless-steel sample holder to grip two collagen samples (3 cm long, 0.5 cm width, and ~ 1 mm thick). The initial distance between the two grips was 2 cm. The direction of the mechanical loading is indicated by red arrows. b) A customized BiSlide module to apply tensile stress to samples during mineralization. c) The sample holder placed on the stage for SAXS measurements at the Advanced Photon Source sector 12-ID-B (Argonne National Laboratory, IL, USA). d) A schematic of SAXS measurement and an example of 2-dimensional intensity data. k_i and k_f are the incident and scattered wave vectors, respectively, and $2\theta_f$ is the exit angle of the X-rays.

Table S1. Concentrations (mM) of ionic components of simulated body fluids and human blood plasma.

Solutions	Na ⁺	K ⁺	Mg ²⁺	Ca ²⁺	Cl ⁻	HCO ₃ ⁻	HPO ₄ ²⁻	SO ₄ ²⁻
SBF ⁴	142.0	5.0	1.5	2.5	147.8	4.2	1.0	0.5
m-SBF	142.0	8.0	1.5	6.3	155.3	4.2	2.5	0.5
Human blood plasma ⁵	142.0	5.0	1.5	2.5	103.0	27.0	1.0	0.5

*The pH of m-SBF was adjusted to 7.4 with 50 mM of Tris ((CH₂OH)₃CNH₂) and 1 N HCl. In m-SBF, 10 mg L⁻¹ pAsp and 0.2 g L⁻¹ sodium azide were also added.

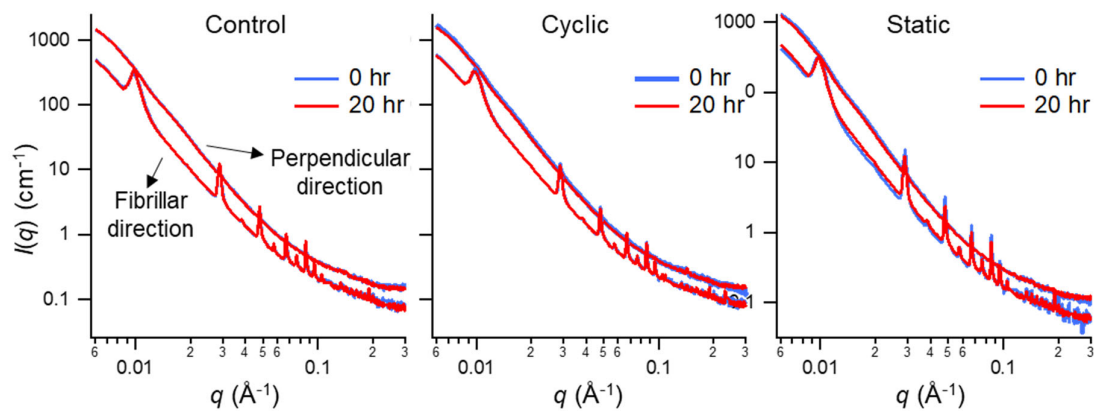


Figure S2. SAXS patterns from collagen matrices before (blue lines) and after (red lines) application of different loading conditions in PBS. 1-dimensional scattering intensities, $I(q)$, were separately extracted for the directions parallel and perpendicular to the fibrillar alignment (Fig. S1d). 1-dimensional $I(q)$ along the fibrillar direction clearly shows several peaks resulted from periodic collagen structures (~ 67 nm). For the other part of the manuscript, 1-dimensional $I(q)$ was extracted along the perpendicular direction to better quantify the nucleation rates and evaluate the morphology of newly formed particles without interference by peaks.

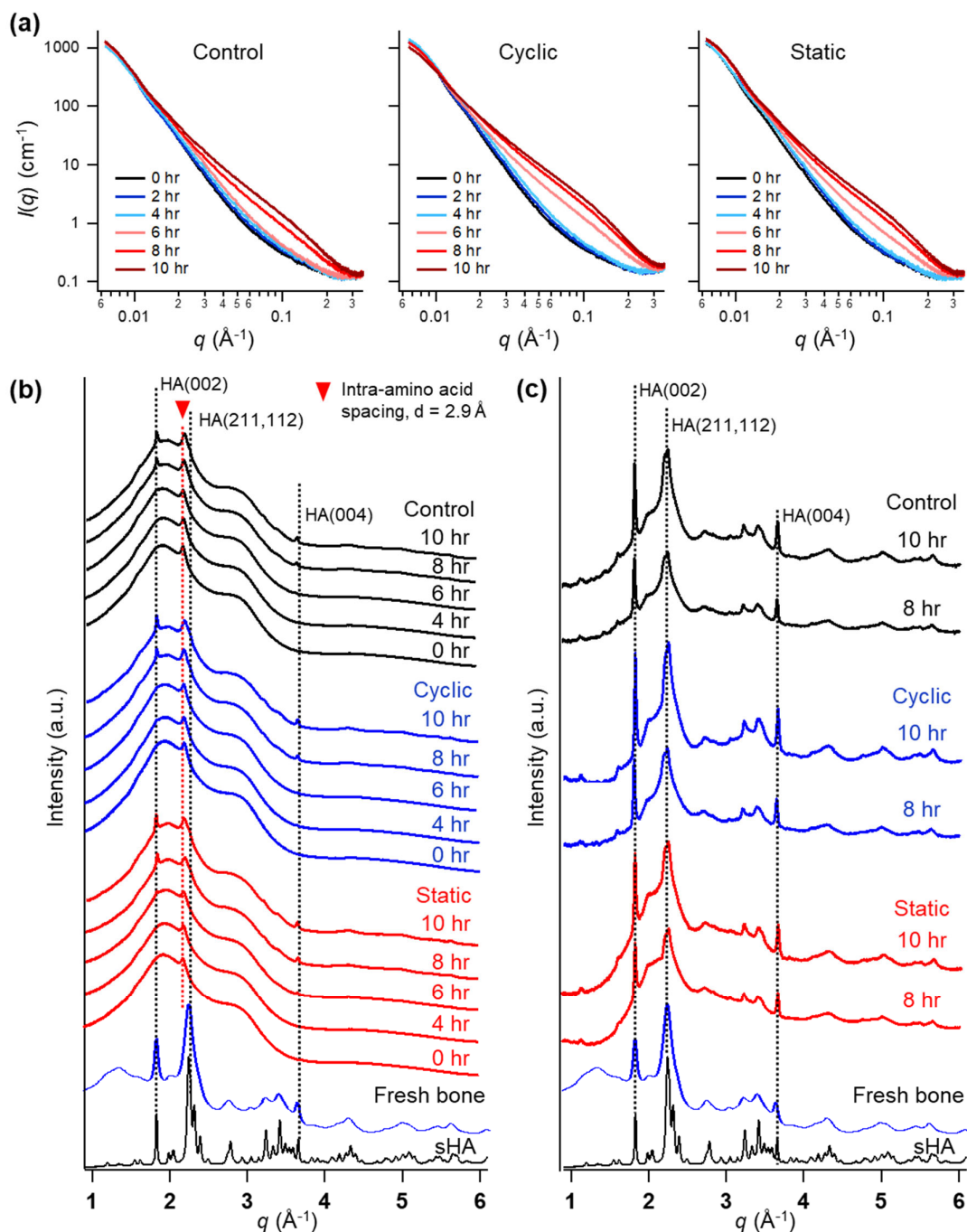


Figure S3. SAXS/WAXD patterns from collagen during mineralization under different strain conditions. a) Examples of *in situ* SAXS evolution of collagen samples during 10 h of mineralization under control, cyclic, and static conditions. b) Raw WAXD patterns showing diffraction from both collagen and CaP nuclei. c) Background-subtracted WAXD patterns showing diffraction only from CaP nuclei. WAXD patterns from a synthetic hydroxyapatite (sHA) and fresh tibia bone are shown for comparison.

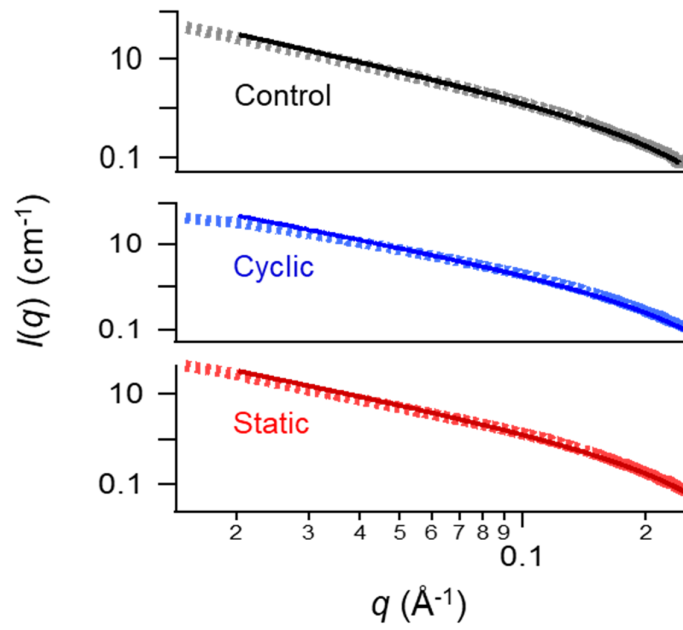


Figure S4. Fitting of background-subtracted SAXS patterns of collagen mineralized for 10 h. Unmineralized collagen data (at 0 h) were used as background patterns. The background-subtracted patterns (dotted lines) fit the plate-like morphology (solid lines, 1.5 nm thick and 40 nm in diameter).

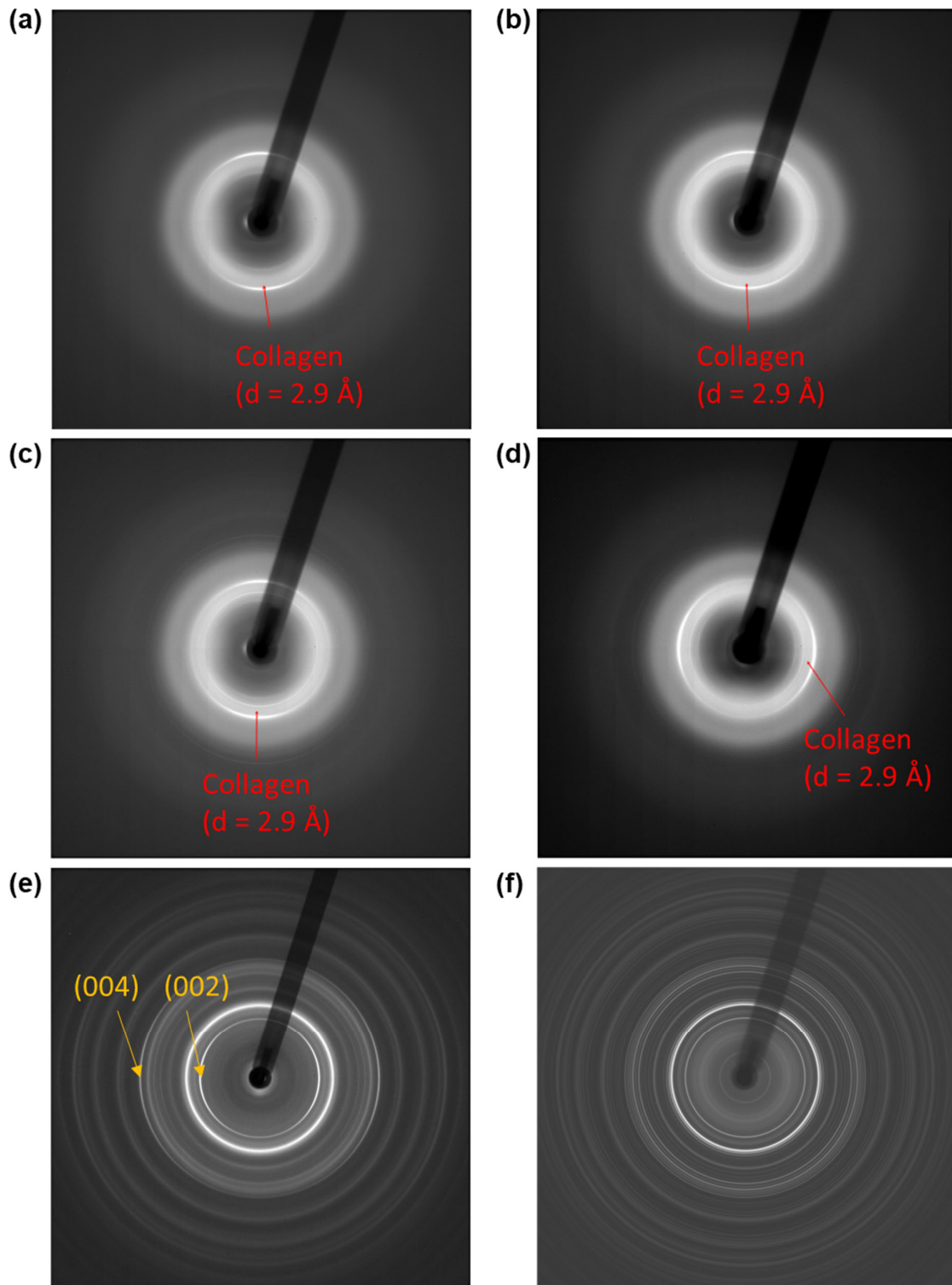


Figure S5. 2-dimensional WAXD images. (a) Unmineralized collagen matrix. (b) Collagen matrix mineralized without strain for 10 h. (c) Collagen matrix mineralized under cyclic strain for 10 h. (d) Collagen matrix mineralized under static strain for 10 h. (e) Fresh fibular bone. (f) Synthetic hydroxyapatite.

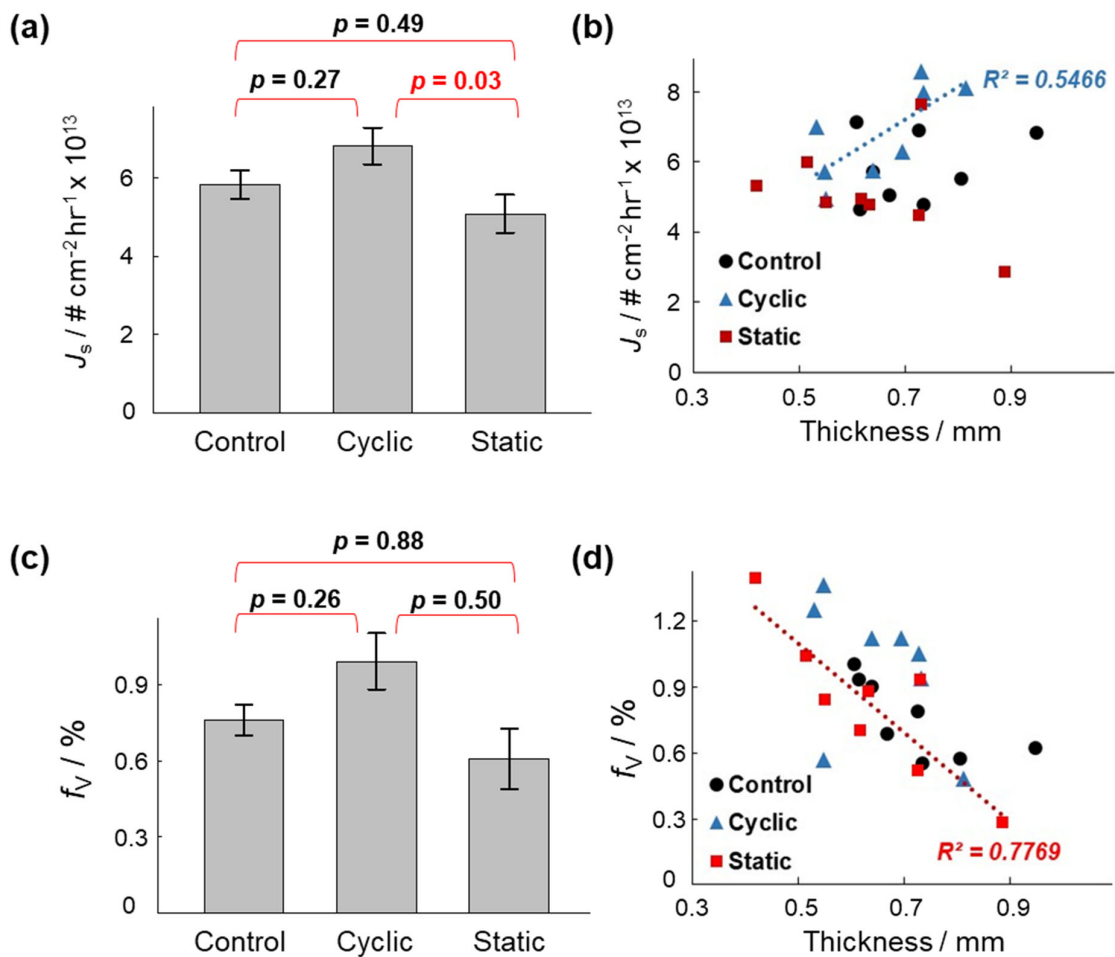


Figure S6. Summary of *in situ* SAXS analysis. (a–b) Nucleation rate per scanning surface area (J_s). (c–d) Volume fraction of CaP nanocrystals in collagen matrix (f_v). The p values were determined using one-way ANOVA with the Tukey HSD post-hoc test.

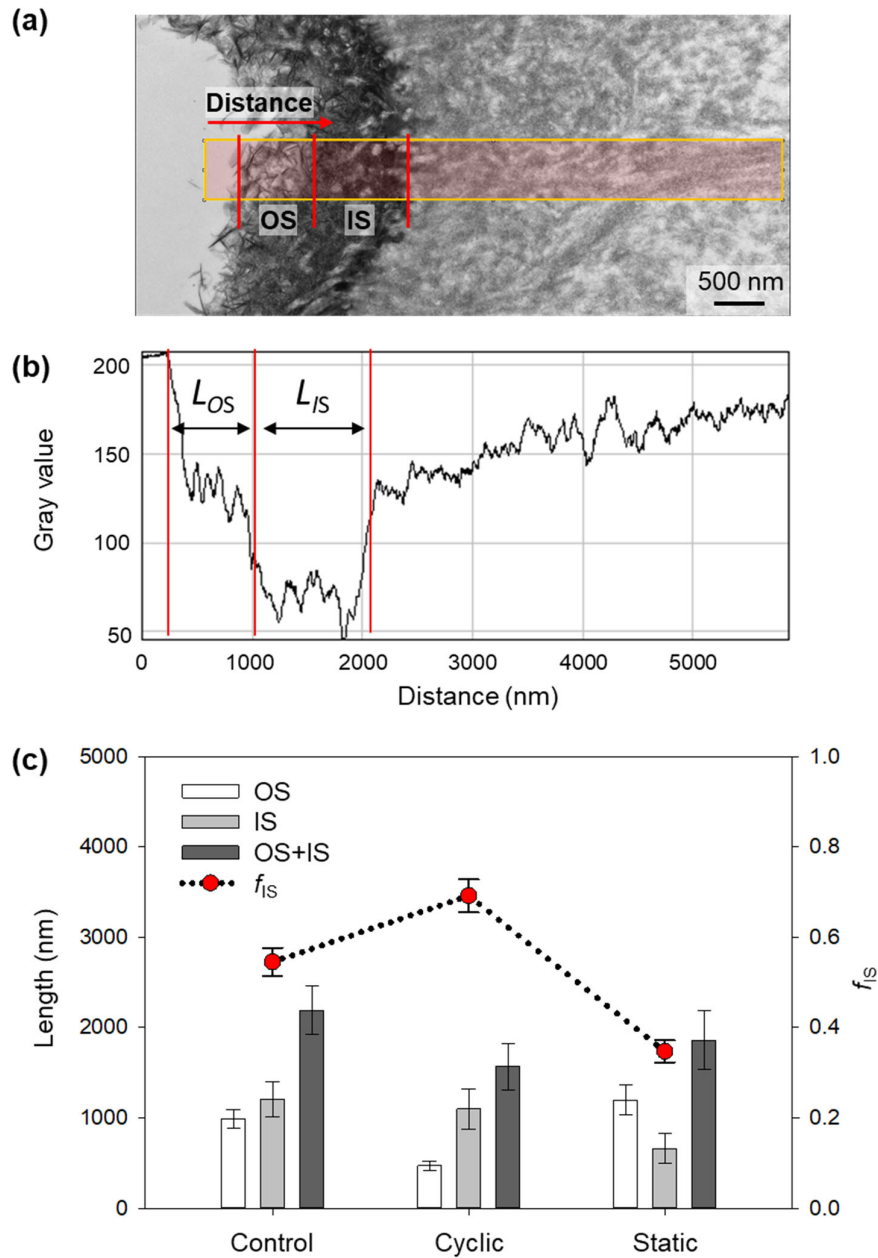


Figure S7. Determination of inner and outer surface mineralization. (a) An example of a selected area (in a highlighted rectangle, ~500 nm thick) for a gray value profile for inner and outer surface mineralization (IS and OS). (b) A gray value profile of the selected area as a function of distance from the outer to the inner surface of the matrix (z -direction in Fig. S5). L_{IS} and L_{OS} are the lengths of IS and OS, respectively. ImageJ software was used for the analysis. (c) Mean and standard errors of L_{IS} , L_{OS} , and their sum in bar graphs obtained from three TEM images per each strain condition. The fraction of inner surface mineralization, f_{IS} (shown in a scattered plot with a dotted line) was calculated by $L_{IS} / (L_{IS} + L_{OS})$. Statistically significant differences in f_{IS} were observed among all groups ($p < 0.05$, one-way ANOVA with the Tukey HSD post-hoc test).

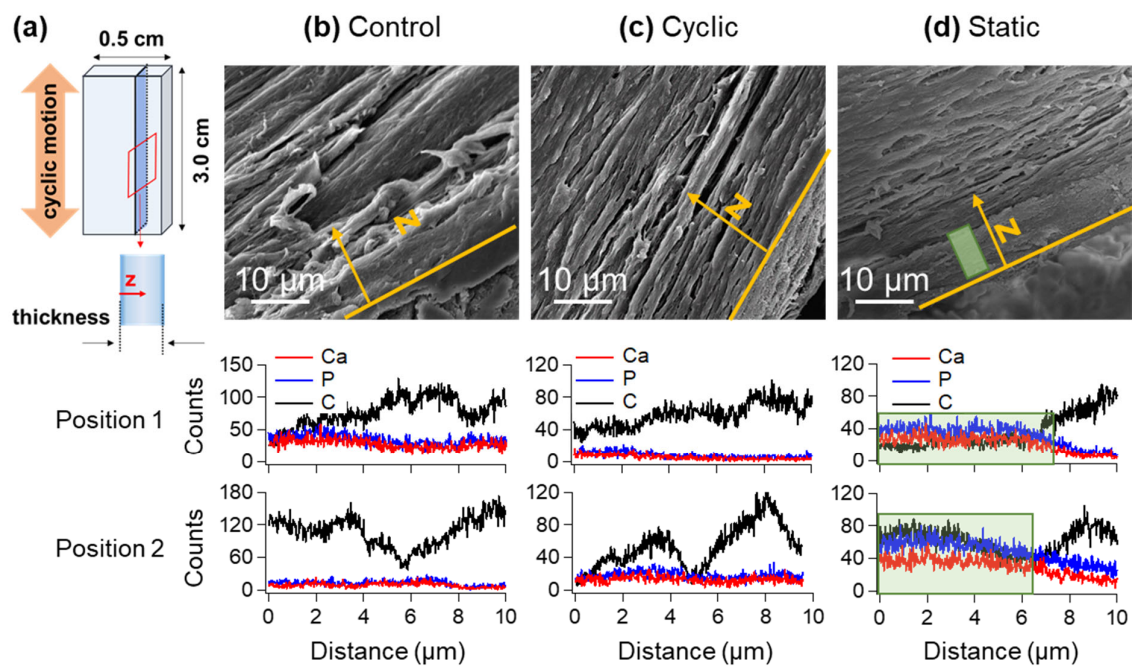


Figure S8. Cross-sectional images of collagen matrices. (a) Schematic of the sample geometry, showing the direction of the cyclic motion. The z -direction indicates the depth of collagen matrices from the outermost surface. (b–d) Scanning electron microscope (SEM) images of cross-sections. Line profiles of elemental composition along the z -direction were obtained from energy-dispersive X-ray spectroscopy (EDX).

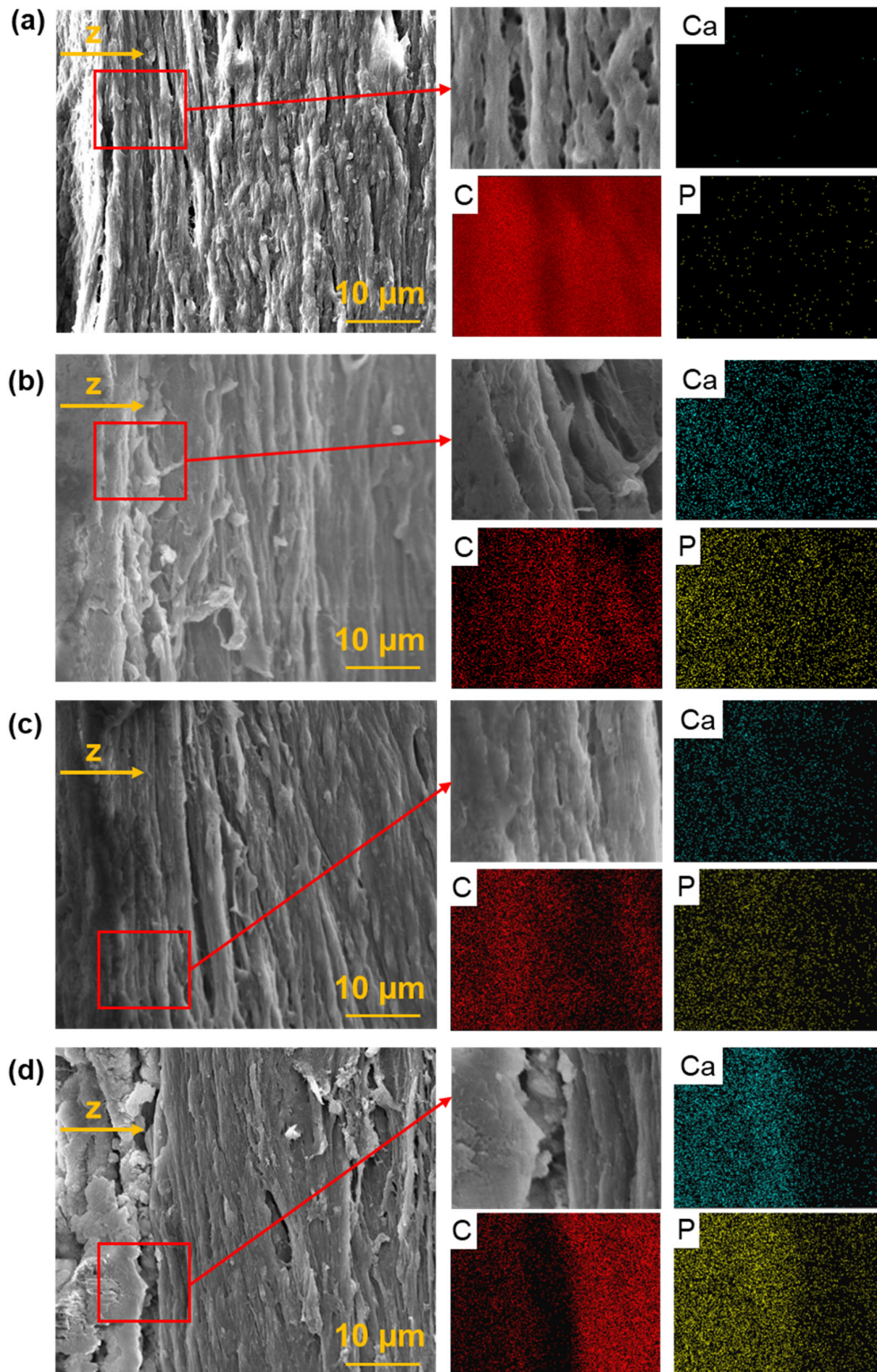


Figure S9. SEM-EDX mapping of cross-sections of collagen matrices. (a) Unmineralized collagen. (b) Control. (c) Cyclic strain. (d) Static condition. The z -direction indicates the depth direction of the matrix. Selected areas of SEM images were analyzed for C, Ca, and P distribution maps.

Table S2. Mechanical and chemical properties of animal bones.

Species	Bone	n^a	E^a (GPa)	m_{Ca}^a (mg g ⁻¹)	Porosity*	f_V^b (%)
Alligator	Femur	9	13.0	253	0.057	40.1
Atlantic whale	Rib	7	8.4	253	0.31	29.4
Axis deer	Term fetus	4	13.2	242	-	36.5
	Mother	3	31.6	274	-	41.3
Bovine	Femur (9 yr)	10	24.5	271	0.044	45.4
	Tibia (1 yr)	8	20.4	252	-	38.0
Brown bear	Femur	3	16.9	255	-	38.4
Crane	T-metatarsus	2	23.1	240	-	36.2
	Tibiotarsus	5	17.6	224	-	33.8
	Ossified tendon	5	22.6	256	-	38.6
Donkey	Radius	7	16.2	255	0.066	40.2
Dugong	Scapula	6	5.5	258	-	38.9
	Radius	2	7.5	253	-	38.1
	Ulna	1	4.9	242	-	36.5
Fallow deer	Tibia	9	25.2	260	0.024	43.4
	Radius	4	25.0	249	-	37.5
Flamingo	Tibiotarsus	4	28.4	257	-	38.7
Galapagos tortoise	Femur	10	12.3	244	0.058	37.9
	Tibia	3	13.0	232	-	35.0
	Fibula	5	11.8	230	0.058	34.6
Man	Femur (3 yr)	7	7	227	-	34.2
	Femur (5 yr)	4	12.8	222	-	33.5
	Femur (35 yr)	4	16.7	249	-	37.5
Horse	Femur (7 yr)	7	23.7	263	0.033	43.8
King penguin	Humerus	4	22.2	266	0.089	42.0
	Radius	2	22.2	265	-	39.9
	Ulna	2	21.7	266	-	40.1
Leopard	Femur	4	21.5	254	-	38.3
Polar bear	Femur (Very Young)	5	8.1	244	-	36.8
	Femur (Young)	13	16.1	259	-	39.0
	Femur (Adult)	6	22.2	268	-	40.4
Red deer	Antler	42	7.1	213	0.134	28.5
Reindeer	Antler	14	7.0	217	0.176	27.8

Rhinoceros	Humerus	9	13.1	253	-	38.1
Roe deer	Femur	5	17.2	259	0.047	42.1
Wallaby	Femur	3	22.0	274	0.032	46.8
	Tibia	4	25.4	268	-	40.4
Walrus	Humerus	5	14.2	245	-	36.9

a) Number of samples (n), elastic modulus (E in GPa), and calcium contents (m_{Ca} in mg g^{-1}) were obtained from Currey *et al.* (2004).⁶ Porosity data were obtained from Currey *et al.* (1988).⁷

b) Volume fraction of mineral, f_V were calculated based on Ca contents based on Equation S1, if porosity data were given.

$$\begin{aligned}
 f_V &= \left(\frac{V_{\text{apatite}}}{V_{\text{apatite}} + V_{\text{collagen}}} \right) \times (1 - \text{porosity}) \\
 &= \left(\frac{m_{\text{apatite}}/\rho_{\text{apatite}}}{m_{\text{apatite}}/\rho_{\text{apatite}} + m_{\text{collagen}}/\rho_{\text{collagen}}} \right) \times (1 - \text{porosity}) \quad (\text{S1})
 \end{aligned}$$

Apatite mineral contents (m_{apatite} in mg g^{-1}) were calculated by assuming all Ca exist as apatite ($\text{Ca}_5(\text{PO}_4)_3\text{OH}$) as written in Equation S2.

$$m_{\text{apatite}} = m_{Ca} \times \frac{MW_{\text{apatite}}}{5 \times MW_{Ca}} \quad (\text{S2})$$

Collagen contents (m_{collagen} in mg g^{-1}) were calculated to be $1 - m_{\text{apatite}}$. For the densities of apatite and collagen (ρ_{apatite} and ρ_{collagen}), 3.16 and 1.35 g cm^{-3} were used, respectively.⁸

When porosity data were not available, f_V were obtained from Equation S3 using an approximate density of bone ($\rho_{\text{bone}} = 1.9 \text{ g cm}^{-3}$), which is relatively constant for most of compact bones.⁹

$$f_V = m_{\text{apatite}} \times 10^{-3} \times \frac{\rho_{\text{bone}}}{\rho_{\text{apatite}}} \quad (\text{S3})$$

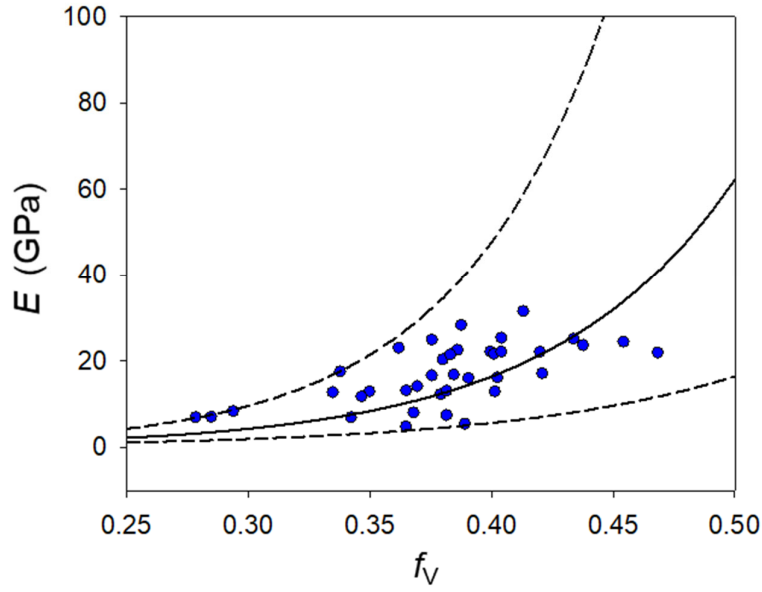


Figure S10. The relationship between E vs. f_V in animal bones. Experimental data (blue dots) obtained from Table S2†. The data were fitted to the equation $\frac{E}{E_{UN}} = \exp(A f_V (1 - 2f_{DP}))$. A is a constant related to the ratio of the elastic moduli of apatite and collagen, and f_{DP} is the fraction of debonded particles. $A = 15.98$ and $f_{DP} = 0.083$ were obtained from the least-square error method for fitting (solid line). All the data were within the range of $\pm 20\%$ of A (dashed lines). The elastic modulus of unmineralized collagen, $E_{UN} = 79.6$ MPa, was obtained from the tensile test results of the PBS group in Fig. 2a of the main text.

References for ESI

- 1 F. Zhang, J. Ilavsky, G. G. Long, J. P. G. Quintana, A. J. Allen and P. R. Jemian, *Metall. Mater. Trans. A*, 2010, **41**, 1151–1158.
- 2 J. Ilavsky and P. R. Jemian, *J. Appl. Crystallogr.*, 2009, **42**, 347–353.
- 3 B. H. Toby and R. B. Von Dreele, *J. Appl. Crystallogr.*, 2013, **46**, 544–549.
- 4 C. Ohtsuki, T. Kokubo and T. Yamamuro, *J. Non. Cryst. Solids*, 1992, **143**, 84–92.
- 5 J. L. Gamble, *Chemical anatomy physiology and pathology of extracellular fluid: A lecture syllabus*, (Harvard University Press) .
- 6 J. D. Currey, *J. Biomech.*, 2004, **34**, 549–556.
- 7 J. D. Currey, *J. Biomech.*, 1988, **21**, 131–139.
- 8 X. Yu, Z. Xia, L. Wang, F. Peng, X. Jiang, J. Huang, D. Rowe and M. Wei, *J. Mater. Chem.*, 2012, **22**, 9721–9730.
- 9 J. R. Cameron, J. G. Skofronick, R. M. Grant and R. L. Morin, *Med. Phys.*, 2000, **27**, 425.